Published in final edited form as:

J Immunol. 2015 June 15; 194(12): 5789–5800. doi:10.4049/jimmunol.1402180.

Programmed death-1 controls T cell survival by regulating oxidative metabolism[1]

Victor Tkachev[*], **Stefanie Goodell**[*], **Anthony W. Opipari**[†], **Ling-Yang Hao**[‡], **Luigi Franchi**[‡], **Gary D. Glick**[§], **James L.M. Ferrara**[*], and **Craig A. Byersdorfer**[¶]

[*]Department of Pediatrics, University of Michigan, Ann Arbor, MI 48109

[†]Department of Obstetrics and Gynecology, University of Michigan, Ann Arbor, MI 48109

[‡]Lycera Corporation, 2800 Plymouth Rd, Ann Arbor, MI 48109

[§]Department of Chemistry, University of Michigan, Ann Arbor, MI 48109

[¶]Division of Blood and Marrow Transplant and Cellular Therapies, Department of Pediatrics, University of Pittsburgh School of Medicine, Pittsburgh PA 15224

Abstract

The co-inhibitory receptor programmed death-1 (PD-1) maintains immune homeostasis by negatively regulating T cell function and survival. Blockade of PD-1 increases the severity of graft-versus-host disease (GVHD), but the interplay between PD-1 inhibition and T cell metabolism is not well studied. We found that both murine and human alloreactive T cells concomitantly up-regulated PD-1 expression and increased levels of reactive oxygen species (ROS) following allogeneic bone marrow transplantation. This PD-1^{Hi}ROS^{Hi} phenotype was specific to alloreactive T cells and was not observed in syngeneic T cells during homeostatic proliferation. Blockade of PD-1 signaling decreased both mitochondrial H_2O_2 and total cellular ROS levels and PD-1 driven increases in ROS were dependent upon the oxidation of fatty acids, as treatment with etomoxir nullified changes in ROS levels following PD-1 blockade. Downstream of PD-1, elevated ROS levels impaired T cell survival in a process reversed by anti-oxidants. Furthermore, PD-1 driven changes in ROS were fundamental to establishing a cell's susceptibility to subsequent metabolic inhibition, as blockade of PD-1 decreased the efficacy of later F_1F_0-ATP synthase modulation. These data indicate that PD-1 facilitates apoptosis in alloreactive T cells by increasing reactive oxygen species in a process dependent upon the oxidation of fat. In addition, blockade of PD-1 undermines the potential for subsequent metabolic inhibition, an important consideration given the increasing use of anti-PD-1 therapies in the clinic.

[1]This work was supported by grants from the National Institute of Health 5PO1-CA039542, RO1-AI47450 (to G.D.G.), and the American Cancer Society (115947-CRP-08-224-01-LIB). C.A.B. was supported by a NIH-sponsored Child Health Research Centers grant (5K12-HD028820) and a Hyundai Hope on Wheels foundation grant.

[2]Corresponding author: Dr. Craig A. Byersdorfer, Division of Blood and Marrow Transplant and Cellular Therapies, Rangos Research Building, 4401 Penn Ave, Pittsburgh, PA 15224, Phone: 412.692.6664, Fax: 412.692.7816; craig.byersdorfer@chp.edu.

Conflict-of-interest disclosure: The remaining authors declare no competing financial interests.

Introduction

T cell activation represents an intricate combination of pro- and anti-stimulatory signals and cells must integrate inputs from multiple co-receptors to initiate and maintain an immune response (1, 2). The co-inhibitory receptor programmed death-1 (PD-1) is a member of the CD28-superfamily and works in concert with its ligands, PD-L1 and PD-L2, to negatively regulate T cell functions including proliferation, cytokine secretion and survival (3). PD-1 signaling is essential for maintaining lymphocyte homeostasis by preventing immune-mediated damage and inducing T cell exhaustion to chronically exposed antigens in infectious and tumor models (4–8). PD-1 is also up-regulated after acute activation, where it helps to dampen the initial T cell response to robust stimulation (9).

PD-1 was first discovered as a marker of apoptosis (10) and recent applications have used PD-1 blockade to enhance T cell responses in a number of therapeutic areas (11–13). Of particular interest, blockade of the PD-1 pathway is being used to increase anti-tumor immunity in patients with advanced stage cancers (4, 11, 13). However, augmenting T cell responses via PD-1 inhibition may have unintended consequences including devastating immune reactions to routine infections (4, 5, 14, 15) and an increased prevalence of autoimmunity (6, 7, 16, 17). In graft-versus-host disease (GVHD), it is well known that absence of PD-1 signaling results in increased IFN-gamma production and lethal immunopathology (18), likely through increased alloreactive T cell expansion and heightened Th1 differentiation (19). Recently, it has been suggested that PD-1 also facilitates changes in alloreactive T cell metabolism (20). However, the detailed mechanisms driving these metabolic changes in alloreactive cells remain incompletely understood. In addition, how PD-1 blockade affects a cell's later ability to respond to subsequent metabolic modulation has not been explored.

In T cells, reactive oxygen species (ROS) are generated as a by-product of mitochondrial respiration, which is tightly coupled to a cell's metabolic status (21, 22). During GVHD, T cells increase mitochondrial respiration, fatty acid oxidation (FAO), and ROS production (23, 24). Increased ROS levels produced during GVHD render T cells susceptible to inhibitory modulation of the F_1F_0-ATP-synthase complex (23) and can also mediate T cell apoptosis (25, 26). Based upon these data, we hypothesized that PD-1 modulates apoptosis in alloreactive T cells by influencing generation of ROS through control of oxidative metabolism. To test this hypothesis, we used genetic and pharmacologic blockade of PD-1 to directly investigate the relationship between PD-1, oxidative metabolism, ROS levels and apoptosis in alloreactive T cells. We find that PD-1 regulates cellular ROS and oxidative metabolism in a process sensitive to inhibition of FAO. Furthermore, blockade of PD-1, which decreases ROS levels, lowers the susceptibility of cells to subsequent metabolic inhibition. These findings have important implications for understanding PD-1 biology and for the use of PD-1 based therapeutics.

Materials and Methods

Mice

Female C57Bl/6 (B6: H-2^b, CD45.2^+, hereafter simply B6), B6-Ly5.2 (H-2^b, CD45.1^+), C57Bl/6×DBA2 F1 (B6D2F1: H-$2^{b/d}$) and Balb/C (H-2^d, CD90.2) mice were purchased from Charles River Laboratories. C3H.HeJ (H-2^k), C3H.SW (H-2^b, Ly9.1^+), C57Bl/6-CAG.OVA (CAG-OVA), CBy.PL(B6)-Thy1^a (Balb/C congenic with CD90.1), and NOD-*scid* IL2Rgamma^{null} (NOD.Cg-Prkdc^{scid}Il2rg^{tm1Wjl}/SzJ) mice were obtained from Jackson Laboratories. Rag1-deficient OT-I and OT-II mice were purchased from Taconic. PD-1 and PD-L1 knockout (KO) mice on a B6 background were provided by Dr. Arlene Sharpe (Harvard Medical School) and have been previously described (17, 27). B6 mice were used as controls. Donor and recipient mice were 8–16 weeks of age at the time of transplantation and cared for according to the Guidelines for Laboratory Animal Medicine at the University of Michigan.

BMT/Cellular Immunization

All recipient mice were conditioned with total body irradiation (^{137}Cs source) on day -1, followed by injection of bone marrow +/− T cells 24 hours later (day 0). Unless stated otherwise, donor cells were positively selected using CD90-magnetic beads (Miltenyi Biotech) according to manufacturer's instructions. For B6 into F1 MHC-mismatched BMT, B6D2F1 mice were conditioned with 1250 cGy TBI in a split dose followed by i.v. infusion of 5×10^6 B6 BM cells and $1–3\times10^6$ T cells from B6-Ly5.2 or PD-1 KO mice. For the Balb/C into B6 model, B6 or PD-L1 mice were conditioned with 1100 cGy (single dose) and received 10×10^6 spleen cells from CBy.PL(B6)-Thy1^a mice plus 5×10^6 Balb/C BM cells. For C3H/HeJ into B6 model, B6-Ly5.2 mice were conditioned with 1000 cGy (single dose) and received 0.5×10^6 C3H.HeJ T cells plus 5×10^6 T-cell depleted C3H/HeJ BM cells. For B6 into Balb/C model, Balb/C mice were conditioned with 800 cGy in a split dose followed by infusion of 5×10^6 B6 BM cells and 1×10^6 B6-Ly5.2 or PD-1 KO T cells.

For C3H.SW into B6 miHC-mismatched transplant, B6 or PD-L1 KO mice were conditioned with 1050 cGy (single dose) and received 5×10^6 C3H.SW BM cells plus C3H.SW T cells at 5×10^6 (WT recipients) or 2×10^6 (PD-L1 KO recipients). For B6 into C3H.SW model, C3H.SW mice were conditioned with 1100 cGy TBI (single dose) followed by i.v. infusion of 5×10^6 B6 BM and 1×10^6 T cells from B6-Ly5.2 or PD-1 KO donors. In syngeneic BMT, B6 mice were conditioned with 1000 cGy, followed by injection of 5×10^6 B6 BM cells and 3×10^6 B6-Ly5.2 T cells. For antigen-specific GVHD, B6-OVA mice were conditioned with 1000 cGy (single dose) and received 1×10^6 negatively selected OT-I T cells, 2×10^6 OT-II T cells, and 5×10^6 T-cell depleted B6 BM cells.

For cellular immunization, B6-Ly5.2 mice were injected with 1×10^6 negatively selected OT-I T cells and 2×10^6 OT-II T cells on day -1. One day later, recipients were injected i.v. with either 1×10^6 positively-selected CD11c cells from B6-OVA mice or 1×10^6 CD11c cells from B6 mice pulsed for 60 minutes with 30 mM ovalbumin. Positive and negative selection of donor T cells and CD11c cells was performed using magnetic separation according to manufacturer's instructions (Miltenyi).

In some experiments, donor T cells were labeled with CellTrace Violet (Molecular Probes) prior to transplant according to manufacturer's instructions. Transplanted mice were housed in sterile, microisolator cages and were given either autoclaved hyperchlorinated (pH 3.0) drinking water (B6, C3H.SW, and F1 recipients), or water supplemented with 0.5 mg/ml Neomycin sulfate and 12.8 μg/ml Polymixin B (Balb/C BMT recipients), for 3 weeks after transplantation. Post-BMT mice were weighed twice weekly and assessment of clinical score was performed weekly as previously described (28).

Xenogeneic GVHD

PBMCs were obtained from healthy volunteer donors according to an IRB-approved consent protocol licensed to the Lycera Corporation, isolated by gradient centrifugation, and labeled with CellTrace Violet. NSG mice were injected with 10^7 human PBMC and each recipient mouse received PBMC from a single, individual donor similar to previously published studies (29, 30). In some experiments NSG mice were conditioned on day -1 with 240 cGy TBI (^{137}Cs source). Splenocytes were harvested between day 12 and day 14, stained for human CD3, CD8, and PD-1 and assessed for ROS levels.

Mouse MLR

5×10^4OT-I T cells or 10^5 B6-Ly5.2 or PD-1KO T cells were negatively-selected from naïve animals, labeled with CellTrace Violet, and cultured for 72 hours with 3×10^5 CAG-OVA or B6D2F1 splenocytes, respectively. MLRs were performed in 96-well flat-bottom plates (Corning) in DMEM (HyClone) supplemented with 10% FBS (GemCell), L-Glutamine, non-essential amino acids, sodium pyruvate, and penicillin/streptomycin (all from Gibco).

Human MLR

Peripheral blood mononuclear cells (PBMCs) from healthy volunteers were enriched by gradient centrifugation using lymphocyte separation medium (Corning). T cells were then negatively selected using the bead-based Pan T cell isolation kit II (Miltenyi) and labeled with CellTrace Violet. Non-T cell fractions of PBMCs were eluted off the column and treated with 25 μg/ml mitomycin C for 45 minutes at 37 °C. T cells were then co-cultured with non-T PBMCs from unrelated donors in AIM-V culture media (Gibco) for 6 days. Anti-human PD-1 blocking antibodies (Clone J116; BioXCell) or anti-PD-L1 blocking antibodies (Clone 19E.2A3; Biolegend) were added at a final concentration of 20 μg/ml or 10 μg/ml, respectively, on day 0, 3 and 6 of culture.

Anti-PD-1/PD-L1 antibody treatment *in vivo*

For PD-L1 blockade, transplant recipients received 200 μg of clone 10F.9G2 (or Rat IgG2b (clone LTF-2)) and for PD-1 blockade, 250 μg of clone RMP1–14 (control = Rat IgG2a (Clone 2A3)) on days 0, 3 and 6 post-BMT. For PD-L2 blockade, animals received clone TY25 (control = Rat Ig2a (2A3)) at 200 μg/dose on a similar dosing schedule. All blocking antibodies were purchased from BioXCell.

LYC-31138 treatment

For BMT survival experiments, F_1F_0-ATPase modulator LYC-31138 was dissolved in vehicle (5% solutol/20% labrafil/ 75% carboxymethylcellulose (0.5% in PBS)) and administered by oral gavage beginning on day 5 post-BMT at 30 mg/kg every other day for a total of 9 doses. LYC-31138 treatment following DC immunization was begun on day +1 and continued for a total of 4 doses. As a control for all LYC-31138 experiments, mice were administered vehicle only (5% solutol/20% labrafil/75% carboxymethylcellulose) on the same dosing schedule. To measure apoptosis and ROS following LYC-31138 treatment, a single dose was administered and splenocytes harvested 2.5 hours later (when the drug had reached maximal serum concentration).

Manganese(III) tetrakis(5,10,15,20-benzoic acid)porphyrin chloride (MnTBAP) and N-acetyl cysteine (NAC) treatment

MnTBAP was dissolved in 0.1N NaOH as 28 mM stock, filtered through 0.1 μM membranes, and finally diluted in sterile PBS to be given at 10 mg/kg. Recipient mice received a single dose of MnTBAP on day 7 post-BMT (for apoptosis measurements) or 5 daily doses of MnTBAP starting on day 8 (for clinical scoring). As a control, recipients received sterile PBS. For *in vitro* antioxidant treatment, MnTBAP or NAC was added into MLR cell media at 24 hours to a final concentration of 100 μM and 10 mM, respectively.

Flow cytometry

Flow cytometry was performed according to previous reports following generation of a single-cell suspension (24). Unless otherwise noted, all antibody and streptavidin staining was carried out on 10^6 cells for 15 minutes at 4 C in in PBS with 2% fetal bovine serum (FBS). To measure total or mitochondrial ROS, cells were stained for surface markers, then loaded with 5 μM CellROX Deep Red (Molecular Probes) or 10 μM MitoPY1 (Tocris) in HBSS containing 2.5 mM of probenecid (Molecular Probes) followed by incubation for 30 minutes at 37°C. Following incubation, cells were washed twice, kept ice-cold in HBSS/ probenecid, and analyzed immediately. To measure superoxide production, cells were incubated with 2.5 μM DHE (Molecular Probes) in HBSS for 30 minutes at 37°C followed by two washes and immediate analysis similar to CellROX and MitoPY1. For measurement of mitochondrial potential ($\Delta\psi_{Mt}$), antibody-stained cells were placed in 40 nM TMRM suspended in phenol red-free DMEM supplemented with 5% FBS, L-glutamine, sodium pyruvate and non-essential amino acids. Cells were incubated with TMRM for 30 minutes at 37°C. Staining was quenched by placing samples on ice and $\Delta\psi_{Mt}$ was immediately assessed. To measure total and respiring mitochondrial mass, cells were stained for cell surface markers, then incubated with 50 nM MitoTracker Green and/or 5 nM MitoTracker DeepRed (both from Molecular Probes) in PBS with 10% FBS for 30 minutes at 37°C. After incubation, cells were washed twice and kept on ice in PBS with 10% FBS until analysis. Apoptosis was measured using AnnexinV-APC in 1× AnnexinV staining buffer according to manufacturer's instructions (BD Biosciences). For intracellular IFN-γ and TNF-α staining, splenocytes were incubated for 6 hours on 96-well plates coated with 2.5 ug/ml CD3/CD28 antibodies (eBioscience), in the presence of 1 μM Brefeldin A. Cells were then stained for membrane antigens, fixed and permeabilized using FoxP3 fixation/permeabilization kit

(eBioscience), and stained with anti-cytokine antibodies for 40 minutes at 4°C. For granzyme B (GzmB) and GLUT1 detection, spleen cells were stained for surface antigens, fixed/permeabilized and stained with PE-conjugated anti-GzmB antibodies or unlabeled rabbit anti-mouse GLUT1 antibody followed by APC-conjugated goat anti-rabbit IgG Fab fragment. Flow cytometry data was acquired using FACSCanto II flow cytometer (BD Biosciences) and analyzed using FlowJo software, version 7.6.1 (Tree Star).

OCR and ECAR measurement

OCR and ECAR values were measured using a Seahorse XF24 metabolic analyzer. Briefly, donor T cells were purified from B6 into F1 recipients on day 7 post-BMT using bead-based negative selection. Cell suspensions were pretreated with 100 μM Etomoxir (or PBS control) for 15 minutes followed by plating unto XF24 plates (Seahorse Bioscience) coated with 0.5 mg/ml poly-D lysine (Sigma). $7–8\times10^5$ cells per well were plated on XF24 plate (Seahorse Bioscience) pre-coated with 0.5 mg/ml poly-D lysine (Sigma). Cells were maintained in XF media (Seahorse Bioscience) supplemented with 1mM sodium pyruvate (Sigma), 11mM glucose (Sigma), and 1% FBS. 100ul of cells were spun down unto poly-D lysine coated plates and 530ul of XF media was added to each well, followed by incubation for 30 minutes in CO_2-free incubator at 37°C. Seahorse analyzer was then run per manufacture's protocol with oligomycin (1uM), FCCP (1uM), and antimycin A (1uM) injected through ports A, B, and C respectively.

Statistical Analysis

Graphing and statistical analysis was performed using GraphPad Prism version 5.01 for Windows (San Diego California USA, www.graphpad.com). Bar graphs represent mean ± standard error of the mean (SEM). Unpaired Student's t test with two tails or multiple t test with Holm-Sidak correction (for multiple comparisons) were used for statistical interpretation unless noted otherwise. Paired Student's t test was used to analyze human MLR data and Mantel-Cox log-rank test was utilized for survival curves analysis. $p < 0.05$ was considered statistically significant.

All investigations have been conducted according to the Declaration of Helsinki principles. All animal and human studies have been approved by the appropriate institutional review boards. Written informed consent was received from human participants prior to their inclusion in the study.

Results

T cells increase PD-1 expression during GVHD

We first studied PD-1 expression in T cells during GVHD. In initial experiments, C57Bl/6 (hereafter B6) bone marrow and B6-Ly5.2 ($CD45.1^+$) T cells were transferred to lethally irradiated B6D2F1 recipients as described in Materials and Methods. T cells from syngeneic transplants (B6-Ly5.2 T cells into B6 recipients) served as non-GVHD controls. Donor T cells ($CD45.1^+$, TCR-β^+) were recovered on day 7 post-BMT and analyzed for PD-1 expression by flow cytometry. Well-divided, $CD8^+$ allogeneic T cells up-regulated PD-1 expression, but syngeneic $CD8^+$ T cells did not (Figure 1A–B). PD-1^{Hi} T cells were

exclusively among the well-divided cells and the percentage of PD-1^{Hi} cells increased from day 4 to day 8 post-BMT, then plateaued (Figure 1B). CD4^{+} T cells increased PD-1 levels similarly post-transplant (Supplementary Figure 1A). In contrast to the exhausted phenotype displayed by some PD-1^{Hi} T cells (4, 8), alloreactive, PD-1^{Hi} T cells up-regulated IFN-γ production and increased granzyme B expression (Supplementary Figure 1B).

PD-1 levels correlate with levels of reactive oxygen species

Alloreactive T cells increase superoxide levels during GVHD (23). We therefore asked whether levels of reactive oxygen species (ROS) tracked with PD-1 status by measuring CellROX staining in PD-1^{Lo} versus PD-1^{Hi} donor T cells. Well-divided, PD-1^{Hi} donor T cells had ROS levels >3.5-fold higher than naïve T cells at multiple times post-allogeneic BMT; PD-1^{Lo} cells did not (Figure 1C–E; Supplementary Figure 1C). The superoxide-specific dye dihydroethidium (DHE) demonstrated a similar increase specifically in PD-1^{Hi} T cells (data now shown). We then tested the correlation between PD-1 and ROS in a minor histocompatibility (miH)-mismatched model of GHVD by transplanting C3H.SW T cells into B6 recipients (details in Materials and Methods). PD-1^{Hi} C3H.SW T cells from both CD4 and CD8 subsets also increased ROS levels in this second model (Supplementary Figure 1D). As a control, >95% of syngeneic T cells undergoing lymphopenia-induced proliferation remained PD-1^{Lo} and did not increase ROS levels (Figure 1C–D). A small percentage of well-divided, syngeneic T cells expressed PD-1 (Figure 1A, upper left quadrant (2.83%)) and ROS levels were elevated in these PD-1^{Hi} cells compared to well-divided PD-1^{Lo} cells (Supplementary Figure 1E). However, PD-1 positive cells from syngeneic recipients expressed less PD-1 (based MFI values), and had lower CellROX staining, than PD-1^{Hi} T cells from allogeneic recipients (data not shown).

CellROX staining measures total cellular ROS levels. To test if mitochondrial respiration also correlated with PD-1 expression, we measured mitochondrial membrane potential using TMRM and mitochondrial H_2O_2 levels with the organelle-specific probe MitoPY1(31). Both parameters increased specifically in PD-1^{Hi} T cells (Figure 1F–G), suggesting a contribution from mitochondrial respiration towards total cellular ROS in these cells. We then asked whether ROS production served as a non-specific marker of cellular activation, or specifically tracked with PD-1^{Hi} status. We assessed this by staining for multiple, common activation markers (CD71, CD98, CD69, CD25, CD44 or CD11a) in ROS^{lo} versus ROS^{Hi} T cells (32–37). Roughly 90% of ROS^{Hi} cells expressed PD-1, while only 30% of ROS^{Lo} cells did so, confirming an association between PD-1 and ROS (Supplementary Figure 2A). None of the other activation markers correlated with ROS to this extent (Supplementary Figure 2B–G). In addition, T cell differentiation status did not predict PD-1 status, as both PD-1^{Hi} and PD-1^{Lo} populations exhibited similar effector-like profiles (Supplementary Figure 2H).

PD-1 controls ROS levels in allogeneic T cells

We next explored whether PD-1 directly controlled ROS levels in allogeneic T cells utilizing two different methods to inactivate PD-1 signaling. First, wild-type (WT) or PD-1 knock-out (PD-1KO) (27) T cells were transferred into B6D2F1 recipients and ROS levels quantitated on day 7 post-transplant. ROS levels decreased 2-fold in both CD8 and CD4

PD-1KO cells, despite ROS levels being similar prior to transplant (Figure 2A–B and Supplementary Figure 3A). Mitochondrial H_2O_2 levels followed a similar pattern (Figure 2C). PD-1KO T cells also decreased ROS levels during an *in vitro* mixed leukocyte reaction, with decreases occurring at all cell divisions (Figure 2D), indicating that PD-1 regulates ROS levels independent of cell division status.

To confirm the finding of decreased ROS levels in PD-1KO cells, we next disrupted PD-1 signaling with blocking antibodies against either PD-1 or PD-L1. *In vivo* blockade of PD-L1 reduced ROS levels 2-fold in PD-1^{Hi} T cells, but did not affect ROS levels in PD-1^{Lo} cells (Figure 2E–F). Blocking antibodies against PD-1 had a similar effect (Supplementary Figure 3B) and avoided interrupting PD-L1 interactions with other cell surface molecules (e.g. CD80 (38)). PD-L1 blockade also lowered mitochondrial H_2O_2 levels in PD-1^{Hi} T cells (Figure 2G). Blockade of PD-L2 did not alter ROS levels in alloreactive cells (data not shown).

Our data indicated that PD-1 inhibition decreased ROS levels in alloreactive T cells. In contrast, Saha and colleagues recently demonstrated that superoxide levels did not decrease in Balb/C T cells transplanted into PD-L1 deficient B6 recipients (20). To explore this discrepancy, we repeated PD-1/ROS analysis in the Balb/C into B6 model (details in Materials and Methods). Similar to the findings of Saha et al., ROS levels did not decrease in Balb/C T cells when transferred into irradiated, PD-L1 KO recipients (Supplementary Figure 3D). To determine if one T cell metabolic phenotype was generalizable to most GVHD models, we analyzed ROS changes following PD-1 blockade in multiple additional MHC- and miHC-mismatched strain combinations (summarized in Table I). As an example, C3H.SW T cells transferred into PD-L1 deficient mice (17) decreased both ROS and mitochondrial H_2O_2 levels identically to B6 T cells transferred to F1 recipients (Figure 2H–I). Similar reductions in ROS levels following PD-1/PD-L1 blockade, using both genetic and antibody-driven inactivation, occurred in all additional models examined, including B6 T cells into Balb/C recipients, B6 T cells into C3H.SW recipients, and C3H/HeJ T cells into B6 recipients. Genetic and pharmacologic blockade of PD-1 also drastically exacerbated GVHD severity, as seen in previous studies (18, 20), with PD-1 inhibited cells displaying an activated phenotype similar to that of PD-1-sufficient cells (data not shown).

To determine if PD-1 driven changes in ROS occurred in human T cells, we performed MLRs using human peripheral blood mononuclear cells (PBMCs), followed by analysis of PD-1 and ROS status. As seen in Figure 3A, responding T cells from murine and human MLRs up-regulated PD-1, and in both systems PD-1 expression (PD-1^{Hi} versus PD-1^{Lo}) correlated with ROS level (Figure 3B, Supplementary Figure 3E). Interestingly, in human MLRs, a subset of PD-1^{Hi} cells never divided. These PD-1^{Hi} cells also displayed higher ROS levels compared to non-dividing, PD-1^{Lo} cells (~2-fold, $p<0.001$), further confirming PD-1's regulation of ROS levels independent of cell division status.

To define the *in vivo* correlation between PD-1 and ROS in human T cells, PBMCs from healthy volunteers were labeled with CellTrace, transferred to immunodeficient NOD*scid* IL2Rgamma^{null} (NSG) mice (xenogenic model of GVHD detailed in Materials and Methods (29, 30)), and harvested between day 12 and 14. Human T cells activated *in vivo* up-

regulated PD-1 with increasing cell division (Figure 3C) and PD-1 expression again correlated with ROS levels (Figure 3D). Addition of PD-1 or PD-L1 blocking antibodies to human MLR cultures reduced ROS levels similarly to changes seen in murine PD-1KO T cells (Figure 3E–F, Supplementary Figure 3F). In summary, in multiple *in vivo* animal models, during both murine and human MLRs, and in the course of xenogeneic GVHD, alloreactive T cells up-regulated PD-1 and in all cases, higher PD-1 expression correlated with increased ROS levels. In addition, in every combination attempted save one, blockade of PD-1 decreased levels of reactive oxygen species.

Inhibiting fatty acid oxidation negates PD-1 regulation of ROS levels

We hypothesized that PD-1 increased ROS production in alloreactive T cells by driving enhanced oxidative respiration. In this hypothesis, actively respiring mitochondria would up-regulate their transmembrane potential ($\Delta\psi_{Mt}$), which would slow electron transfer between chain complexes, favoring electron leak and resulting in elevated superoxide formation (39). In support of this, PD-L1 blockade decreased $\Delta\psi_{Mt}$ in allogeneic T cells, without significantly changing their mitochondrial mass (Supplementary Figure 3G). Importantly, changes in ROS levels did not result from mitochondrial damage, as the percentage of cells with damaged mitochondria was similar between isotype and anti-PD-L1 treated animals (data not shown).

We have previously shown that alloreactive T cells rely on fatty acid oxidation (FAO) as a component of oxidative phosphorylation to meet their bioenergetic demands (23, 24). To test the relationship between oxidative metabolism and PD-1, we measured oxygen consumption rates (OCR) in day 7 allogeneic T cells following PD-L1 blockade. Consistent with a reduction in $\Delta\psi_{Mt}$, anti-PD-L1-treated T cells had lower basal OCR (Figure 4A–B). Pre-treatment of alloreactive T cells with etomoxir, an inhibitor of FAO, reduced rates of oxygen consumption and nullified OCR differences between anti-PD-L1 and control treated T cells (Figure 4B and Supplementary Figure 3H). Etomoxir treatment also decreased ROS and mitochondrial H_2O_2 levels and, more importantly, obviated the ability of anti-PD-L1 treatment to lower ROS levels further (Figure 4C–D). PD-L1 blockade increased the extracellular acidification rate (ECAR) of alloreactive T cells, but only when oxidative respiration was inhibited by oligomycin (Figure 4E). This increased ECAR was likely facilitated by increased glucose transport, as GLUT1 levels rose following PD-1 pathway blockade (Figure 4F). In total, these metabolic data demonstrate that in alloreactive T cells, inhibition of FAO negates PD-1 driven changes in oxidative metabolism and ROS levels.

PD-1 induces T cell apoptosis through an ROS-dependent mechanism

While PD-1 is implicated in immune homeostasis and peripheral tolerance (40), it was originally discovered as a marker of lymphocyte apoptosis(10). We therefore probed the relationship between PD-1, ROS, and cell death in alloreactive T cells. PD-1 expression directly correlated with AnnexinV staining in alloreactive cells (Figure 5A), and $AnnexinV^+$ staining decreased after both antibody blockade and genetic disruption of PD-1 (Figure 5B and data not shown). Decreased alloreactive cell death following PD-1 blockade resulted in an increased number of well-divided T cells, a higher proportion of $PD\text{-}1^{Hi}$ cells, and a dramatic exacerbation of GVHD (20). From this data, we posited that PD-1 potentiates

apoptosis through modulation of ROS levels. To test this hypothesis, we treated MLR cultures, or day 7 alloreactive T cells placed *ex vivo*, with the antioxidant manganese(III) tetrakis(5,10,15,20-benzoic acid)porphyrin chloride (MnTBAP) (41, 42), a compound known to protect lymphocytes from ROS-mediated cell death (26). Both MLR cultures and day 7 T cells incubated overnight with MnTBAP (or the structurally-unrelated antioxidant N-acetylcysteine (NAC)) reduced their percentage of AnnexinV^{+} cells (Supplementary Figure 4A–C).

We next confirmed the role of ROS in driving T cell apoptosis *in vivo* by administering MnTBAP to recipients during a miHC-mismatched model of GVHD (C3H.SW into B6). To limit interference with initial priming, we waited to treat recipient mice until day 9 post-transplant with a single dose of MnTBAP (43). MnTBAP treatment reduced the percentage of AnnexinV^{+}, PD-1^{Hi} T cells, but did not alter apoptosis in PD-1^{Lo} lymphocytes (Figure 5C, Supplementary Figure 4D). Cell death was similarly reduced following MnTBAP treatment in a MHC-mismatched model of GVHD (Supplementary Figure 4E) and apoptosis of alloreactive T cells correlated inversely with GVHD severity following serial doses of MnTBAP (Figure 5D). Notably, MnTBAP-treated animals had identical proportions of PD-1^{Hi} T cells, with similar PD-1 MFI (Supplementary Figure 4F), placing MnTBAP's mechanism of action downstream of PD-1 but upstream of cell death. Importantly, MnTBAP treatment had no effect in syngeneic recipients (data not shown).

Stable PD-1^{Hi}ROS^{Hi} phenotype is specific to alloreactive T cells and requires exposure to antigen

To determine if PD-1 regulation of ROS is unique to the GVHD environment, we compared PD-1 expression on alloreactive T cells during GVHD versus T cells responding to cellular immunization. To model GVHD, OT-I T cells (responsive to the SIINFEKL peptide of ovalbumin (OVA)) were transferred into irradiated recipients expressing ubiquitous ovalbumin (B6 CAG-OVA). This model results in classic characteristics of acute GVHD including hunched posture, fur ruffling, decreased mobility, weight loss and 40% lethality by day 30 (data not shown). For cellular immunization, the same OT-I T cells were injected into syngeneic hosts (B6-Ly5.2), followed by intravenous immunization with purified CAG-OVA dendritic cells (24). OT-I T cells transferred into an antigen-driven GVHD environment had robustly up-regulated PD-1 levels by day 7 post-transplant; OT-I cells following dendritic cell immunization did not (Figure 6A). Consistent with a lack of PD-1 up-regulation, OT-I cells on day 7 following cellular immunization did not increase their ROS levels (Figure 6B–C). Absent PD-1 expression was not the result of poor T cell proliferation or aberrant differentiation, as T cells post-immunization divided >8 times by day 7 (Figure 6A), acquired an effector-like phenotype (CD44^{Hi}CD62L^{Lo}), up-regulated Granzyme B expression, and had equivalent IFN-γ upon re-stimulation (data not shown). However, lack of PD-1 up-regulation following immunization contrasted with PD-1 up-regulation observed during acute viral infection (44) or following *in vitro* stimulation of T cells with anti-CD3 antibody (14). To investigate this discrepancy, we tested expression of PD-1 on OT-I cells at an earlier time post-immunization. On day 3 after dendritic cell injection, ~70% of OT-I T cells adopted a PD-1^{Hi} phenotype (Fig 6D) and expression correlated with elevated ROS levels at this earlier point (Fig 6E). Cellular immunization

thus results in limited PD-1 expression, with concomitant increase in ROS levels, consistent with the transient increase in PD-1 observed during an acute viral response (44).

To test whether the inflammatory milieu of GVHD, combined with a lymphopenic environment, might be sufficient to drive adoption of a PD-$1^{Hi}ROS^{Hi}$ phenotype, we co-transferred CD45.1/CD45.2 OT-I T cells and $CD45.1^+$ (B6-Ly5.2) T cells into either irradiated CAG-OVA recipients or B6 syngeneic controls. In the GVHD environment (CAG-OVA recipients), OT-I T cells increased both PD-1 expression and up-regulated ROS levels; B6-Ly5.2 syngeneic T cells recovered from the same animals did not (Figure 6F–G). No differences in PD-1 expression or ROS status were observed in OT-I or B6-Ly5.2 T cells transferred to syngeneic B6 mice. Thus, cell proliferation alone, even in the context of an inflammatory or lymphopenic milieu, is insufficient to drive adoption of a PD-$1^{Hi}ROS^{Hi}$ phenotype.

PD-1 is required for ROS-dependent metabolic inhibition

Compounds that modulate the F_1F_0-ATP synthase complex have potential application as novel therapies for immune-mediated disease (23). These compounds work in part by inducing apoptosis of robustly activated, pathogenic lymphocytes in a manner dependent upon ROS generation (45, 46). Given the increased ROS levels in PD-1^{Hi} T cells, we hypothesized that PD-1^{Hi} T cells would show preferential susceptibility to F_1F_0-ATPase modulators. To test this idea, irradiated B6D2F1 recipients received either wild-type or PD-1KO T cells, followed by a single treatment with the F_1F_0-ATPase modulator LYC-31138 on day 7 post-BMT. LYC-31138 treatment increased both ROS levels and $AnnexinV^+$ staining in WT PD-1^{Hi} T cells, but did not change ROS levels or $AnnexinV^+$ staining in PD-1KO T cells (Figure 7A–B). In addition, LYC-31138-driven apoptosis was obviated by pre-treatment with anti-PD-L1 antibodies (Figure 7C). We next transplanted C3H.SW T cells into WT versus PD-L1 KO recipients in a miHC-mismatched model of GVHD, followed by administration of LYC-31138. In this model, PD-1^{Hi} T cells decreased nearly two-fold in WT recipients following LYC-31138 treatment (Figure 7D), but did not change in number in recipients lacking PD-L1. Consistent with a decrease in donor T cell numbers, LYC-31138 treatment specifically improved survival in WT recipients (Figure 7E), but not in PD-L1KO recipients where PD-1 signaling was abolished (Figure 7F). As expected, donor T cell proliferation, cell number and survival were unchanged by LYC-31138 treatment during syngeneic transplantation or following cellular immunization (data not shown).

In summary, our data demonstrate that PD-1 controls ROS levels and mitochondrial respiration in alloreactive T cells in a process dependent upon FAO and that increases in ROS directly impact T cell survival. In addition, PD-1 blockade, by lowering ROS levels, impairs the potential for subsequent ROS-driven metabolic modulation.

Discussion

PD-1 signaling plays an important role in immune homeostasis, both by dampening an initial T cell response to acute activation (9), and by inducing exhaustion in T cells undergoing chronic exposure to antigen (8). In this way, PD-1 acts as a safeguard against

prolonged and potentially detrimental activation (5–7). During GVHD, PD-1 expression on alloreactive T cells limits the severity of GVHD and lack of PD-1 signaling drives T cell expansion, increases IFN-γ production, and accelerates GVHD onset (18). PD-1 blockade also leads to metabolic changes in alloreactive cells (20), but the mechanisms underlying these metabolic changes have not been well studied and the consequences of PD-1 blockade on subsequent metabolic modulation have not been explored.

Here we demonstrate that alloreactive T cells express high levels of PD-1 early post-transplant, with a phenotype similar to PD-1 expressing T cells recovered during acute viral infections (47, 48). Alloreactive, PD-1^{Hi} T cells also increase cellular ROS levels with a concomitant increase in T cell apoptosis. It is noteworthy that ROS levels do not correlate with expression of other common activation markers, including CD71 and CD98, which are directly linked to T cell metabolism (32). This suggests there is something unique about the coordinated up-regulation of PD-1 and ROS levels. And while ROS levels may correlate with additional members of the CD28-family such as ICOS (49, 50), increased ROS are not simply generic markers of activation. Importantly, the PD^{Hi}, ROS^{Hi} phenotype is not seen in syngeneic T cells, or in well-divided T cells 7 days after cellular immunization. Given the lower levels of fatty acid transport and metabolic co-activators observed in these non-alloreactive cells (24), it is not surprising that ROS levels are lower at the time points examined. For cellular immunization, we speculate that the environment influences this lack of ROS, given that a limited amount of antigen is presented for a finite period of time in the context of nominal systemic inflammation. These limitations lead to only brief stimulation and consequently a transient up-regulation of PD-1 with limited ROS production (51).

Saha and colleagues recently demonstrated a role for PD-1 in controlling alloreactive T cell metabolism in a Balb/C into B6 GVHD model (20). In many respects, our findings complement their report. In both studies, blockade of PD-L1 (but not PD-L2) worsened GVHD and led to a more rapid onset of mortality. However, the response of ROS levels to PD-1 blockade was variable. ROS levels did not decrease in Balb/C T cells transferred to PD-L1 deficient hosts ((20) and Supplementary Figure 3E). In contrast, in all other strain combinations tested, using a variety of donor strains (B6, C3H/HeJ, and C3H.SW T cells), and a number of inactivation strategies, blockade of PD-1 decreased ROS levels and limited T cell apoptosis. We do not have a clear explanation for why Balb/C T cells behave differently than all other alloreactive cells examined, but suspect that the impact of PD-1 on metabolic reprogramming may ultimately depend upon the genetic differences in the strain of the donor T cell (52, 53). Regardless of the reason for the difference, the weight of evidence in Table I demonstrates that in a great majority of alloreactive T cells, PD-1 blockade decreases ROS levels, including in human T cells.

In T cells, ROS can be generated by either NADPH oxidases (e.g. NADPH-oxidase 2 (NOX2), dual-substrate oxidase 1 (DUOX1)) (54–56), or the action of respiring mitochondria, whose function is tightly coupled to a cell's metabolic status (57–59). We observed no change in NOX or DUOX enzyme complexes in alloreactive T cells and ROS levels were insensitive to both NOX2 and DUOX1 inhibition (data not shown). In contrast, mitochondrial respiration likely contributes to PD-1 driven changes in total cellular ROS as a significant correlation exists between total cellular ROS and mitochondrial H_2O_2 levels

(Supplementary Figure 3D). Furthermore, decreases in mitochondrial H_2O_2 mirrored decreases in ROS in PD-1KO T cells (Figure 2B–C), following PD-L1 blockade (Figure 2E–F), in T cells recovered from PD-L1 deficient recipients (Figure 2G–H), and following blockade of FAO with etomoxir (Figure 4C–D). Importantly, PD-1 blockade does not completely prevent ROS generation, as ROS levels in PD-1KO T cells remain 2-fold higher than in un-manipulated T cells (Figure 2). In this context, blockade of PD-1 may simply reduce a portion of ROS (e.g. the ROS generated from FAO), while preserving ROS generation from other internal sources (Figure 4), thus lessening apoptosis while still preserving the physiological levels of ROS critical for T cell activation (58). In addition, the fact that PD-1 blockade modulates ROS levels in PD-1^{Hi} cells, but not in adjacent PD-1^{Lo} cells, suggests that PD-1-dependent regulation of mitochondrial respiration is likely a cell-intrinsic process.

We have previously reported that alloreactive T cells increase superoxide levels during GVHD as a result of increased mitochondrial respiration (23). Here we demonstrate that PD-1 regulates T cell oxygen consumption, mitochondrial H_2O_2 production, and total cellular ROS levels. Our data also suggest that PD-1 driven increases in ROS depend upon FAO, because ROS levels are not additionally susceptible to PD-1 blockade if cells are treated with etomoxir (Figure 4). From this data, we speculate that PD-1 signaling drives T cells towards increased lipid metabolism. During GVHD, intensely activated T cells must choose between glucose and alternative substrates such as fatty acids to meet their bioenergetic demands. PD-1 signaling influences this choice by blocking glucose utilization through restricted Glut1 expression (20, 21), necessitating the up-regulation of alternative energy sources including fat metabolism. When PD-1 signaling is blocked, Glut1 inhibition is released (Figure 4F) and T cells readily up-regulate aerobic glycolysis, particularly when oxidation is compromised (Figure 4E). In support of this proposition, PD-1 also modulates other key regulators of T cell glucose metabolism including both Akt and mTOR signaling (21, 22).

Increased ROS mediate T cell death in numerous systems (25, 26, 55, 60), including through the process of activated T cell autonomous death (ACAD) (25). During ACAD, high ROS levels drive down expression of anti-apoptotic proteins (e.g. Bcl2), facilitating release of intracellular mediators into the cytoplasm (e.g. cytochrome c), ending in apoptotic cell death (61). In the current study, both *in vitro* and *in vivo* antioxidant treatment prevented apoptosis of PD-1^{Hi} T cells, but did not have the same effect on PD-1^{Lo} cells, confirming that ROS are key to carrying out PD-1 induced cell death (Figure 5). We postulate that in alloreactive T cells, ROS levels generated from PD-1 driven increases in oxidative respiration trigger the release of intracellular mediators that then initiate T cell apoptosis. We cannot rule out a role for Fas/FasL-induced apoptosis in the current study (62), but this mechanism seems less likely given that Fas ligand expression was not required for GVHD enhancement in previous studies of PD-1 inhibition (18).

Given the emerging clinical significance of PD-1 blockade as a novel immunotherapy (11, 13), it is extremely important to understand how disruption of PD-1 signaling affects subsequent T cell function. Given their increased oxidative status, we correctly reasoned that PD-1^{Hi} lymphocytes would be preferentially susceptible to F1-F0 ATPase modulation

because of their high ROS levels (Figure 7B). This suggests that augmentation of PD-1 signaling might sensitize cells to ROS-dependent interventions and enhance the efficacy of ROS-targeted therapies. Conversely, as seen in Figures 7D–F, PD-1 blockade renders T cells resistant to future ROS-dependent metabolic inhibition (45, 46), a finding that may have significant clinical implications. For example, adjuvant therapies that depend upon increased ROS levels (e.g. glucocorticoids, methotrexate, and cyclophosphamide (63–65)) will likely exhibit reduced efficacy in T cells following PD-1 blockade. In these situations, use of alternative, ROS-independent therapies (e.g. targeted use of cyclosporine or mycophenolate (66–68)) might be preferred.

In summary, PD-1 controls disease severity in multiple GVHD models by dictating T cell sensitivity to apoptosis through modulation of mitochondrial respiration and subsequent generation of intracellular ROS. Blockade of PD-1 signaling decreases apoptosis and also lessens the susceptibility of T cells to future oxidative manipulation. It is easy to envision how these PD-1 signals might be further exploited to influence immune reactions in a bi-directional manner. Down-regulation of PD-1 could preserve T cell survival by minimizing ROS generation and limiting ROS-driven apoptosis, an important attribute for *in vivo* immunotherapy. In contrast, augmentation of PD-1 signals might increase ROS-dependent apoptosis, thereby serving as a potent treatment for T cell-mediated immune disease, particularly in situations where intracellular ROS levels are already increased. Thus, constructing a detailed understanding of the metabolic effects downstream of PD-1 will remain an important area of future investigation as the clinical use of anti-PD-1 therapies continues to grow.

Supplementary Material

Refer to Web version on PubMed Central for supplementary material.

Acknowledgements

V.T. performed and designed experiments, interpreted all experiments, and wrote the paper, S.G. designed and performed experiments, L.H. designed and interpreted Seahorse analysis, L.F. designed and performed human xenogeneic GVHD experiments, A.W.O. designed and interpreted Seahorse, xenogeneic GVHD, and LYC-31138 experiments, G.D.G. interpreted LYC-31138 experiments and edited the paper, and J.L.F. designed and interpreted all experiments and wrote the paper. C.A.B. designed experiments, interpreted all experiments, and wrote the paper with V.T and J.L.F.

A.W.O., L-Y.H., L.F., and G.D.G. acknowledge employment and financial interest in Lycera, Inc., a private company that has licensed technology from the University of Michigan that may have some relationship to content in this report.

References

1. Lanzavecchia A, Sallusto F. Progressive differentiation and selection of the fittest in the immune response. Nat Rev Immunol. 2002; 2:982–987. [PubMed: 12461571]
2. Chen L, Flies DB. Molecular mechanisms of T cell co-stimulation and co-inhibition. Nat Rev Immunol. 2013; 13:227–242. [PubMed: 23470321]
3. Keir ME, Butte MJ, Freeman GJ, Sharpe AH. PD-1 and its ligands in tolerance and immunity. Annu Rev Immunol. 2008; 26:677–704. [PubMed: 18173375]

4. Barber DL, Wherry EJ, Masopust D, Zhu B, Allison JP, Sharpe AH, Freeman GJ, Ahmed R. Restoring function in exhausted CD8 T cells during chronic viral infection. Nature. 2006; 439:682–687. [PubMed: 16382236]
5. Mueller SN, Vanguri VK, Ha SJ, West EE, Keir ME, Glickman JN, Sharpe AH, Ahmed R. PD-L1 has distinct functions in hematopoietic and nonhematopoietic cells in regulating T cell responses during chronic infection in mice. J Clin Invest. 2010; 120:2508–2515. [PubMed: 20551512]
6. Frebel H, Nindl V, Schuepbach RA, Braunschweiler T, Richter K, Vogel J, Wagner CA, Loffing-Cueni D, Kurrer M, Ludewig B, Oxenius A. Programmed death 1 protects from fatal circulatory failure during systemic virus infection of mice. The Journal of experimental medicine. 2012; 209:2485–2499. [PubMed: 23230000]
7. Frebel H, Oxenius A. The risks of targeting co-inhibitory pathways to modulate pathogen-directed T cell responses. Trends Immunol. 2013; 34:193–199. [PubMed: 23333205]
8. Wherry EJ. T cell exhaustion. Nature immunology. 2011; 12:492–499. [PubMed: 21739672]
9. Freeman GJ, Long AJ, Iwai Y, Bourque K, Chernova T, Nishimura H, Fitz LJ, Malenkovich N, Okazaki T, Byrne MC, Horton HF, Fouser L, Carter L, Ling V, Bowman MR, Carreno BM, Collins M, Wood CR, Honjo T. Engagement of the PD-1 immunoinhibitory receptor by a novel B7 family member leads to negative regulation of lymphocyte activation. The Journal of experimental medicine. 2000; 192:1027–1034. [PubMed: 11015443]
10. Ishida Y, Agata Y, Shibahara K, Honjo T. Induced expression of PD-1, a novel member of the immunoglobulin gene superfamily, upon programmed cell death. EMBO J. 1992; 11:3887–3895. [PubMed: 1396582]
11. Brahmer JR, Tykodi SS, Chow LQ, Hwu WJ, Topalian SL, Hwu P, Drake CG, Camacho LH, Kauh J, Odunsi K, Pitot HC, Hamid O, Bhatia S, Martins R, Eaton K, Chen S, Salay TM, Alaparthy S, Grosso JF, Korman AJ, Parker SM, Agrawal S, Goldberg SM, Pardoll DM, Gupta A, Wigginton JM. Safety and activity of anti-PD-L1 antibody in patients with advanced cancer. N Engl J Med. 2012; 366:2455–2465. [PubMed: 22658128]
12. Pardoll DM. Immunology beats cancer: a blueprint for successful translation. Nature immunology. 2012; 13:1129–1132. [PubMed: 23160205]
13. Topalian SL, Hodi FS, Brahmer JR, Gettinger SN, Smith DC, McDermott DF, Powderly JD, Carvajal RD, Sosman JA, Atkins MB, Leming PD, Spigel DR, Antonia SJ, Horn L, Drake CG, Pardoll DM, Chen L, Sharfman WH, Anders RA, Taube JM, McMiller TL, Xu H, Korman AJ, Jure-Kunkel M, Agrawal S, McDonald D, Kollia GD, Gupta A, Wigginton JM, Sznol M. Safety, activity, and immune correlates of anti-PD-1 antibody in cancer. N Engl J Med. 2012; 366:2443–2454. [PubMed: 22658127]
14. Iwai Y, Terawaki S, Ikegawa M, Okazaki T, Honjo T. PD-1 inhibits antiviral immunity at the effector phase in the liver. The Journal of experimental medicine. 2003; 198:39–50. [PubMed: 12847136]
15. Phares TW, Stohlman SA, Hinton DR, Atkinson R, Bergmann CC. Enhanced antiviral T cell function in the absence of B7-H1 is insufficient to prevent persistence but exacerbates axonal bystander damage during viral encephalomyelitis. Journal of immunology. 2010; 185:5607–5618.
16. Dong H, Zhu G, Tamada K, Flies DB, van Deursen JM, Chen L. B7-H1 determines accumulation and deletion of intrahepatic CD8(+) T lymphocytes. Immunity. 2004; 20:327–336. [PubMed: 15030776]
17. Latchman YE, Liang SC, Wu Y, Chernova T, Sobel RA, Klemm M, Kuchroo VK, Freeman GJ, Sharpe AH. PD-L1-deficient mice show that PD-L1 on T cells, antigen-presenting cells, and host tissues negatively regulates T cells. Proc Natl Acad Sci U S A. 2004; 101:10691–10696. [PubMed: 15249675]
18. Blazar BR, Carreno BM, Panoskaltsis-Mortari A, Carter L, Iwai Y, Yagita H, Nishimura H, Taylor PA. Blockade of programmed death-1 engagement accelerates graft-versus-host disease lethality by an IFN-gamma-dependent mechanism. Journal of immunology. 2003; 171:1272–1277.
19. Sandner SE, Clarkson MR, Salama AD, Sanchez-Fueyo A, Domenig C, Habicht A, Najafian N, Yagita H, Azuma M, Turka LA, Sayegh MH. Role of the programmed death-1 pathway in regulation of alloimmune responses in vivo. Journal of immunology. 2005; 174:3408–3415.

20. Saha A, Aoyama K, Taylor PA, Koehn BH, Veenstra RG, Panoskaltsis-Mortari A, Munn DH, Murphy WJ, Azuma M, Yagita H, Fife BT, Sayegh MH, Najafian N, Socie G, Ahmed R, Freeman GJ, Sharpe AH, Blazar BR. Host programmed death ligand 1 is dominant over programmed death ligand 2 expression in regulating graft-versus-host disease lethality. Blood. 2013; 122:3062–3073. [PubMed: 24030385]
21. Parry RV, Chemnitz JM, Frauwirth KA, Lanfranco AR, Braunstein I, Kobayashi SV, Linsley PS, Thompson CB, Riley JL. CTLA-4 and PD-1 receptors inhibit T-cell activation by distinct mechanisms. Mol Cell Biol. 2005; 25:9543–9553. [PubMed: 16227604]
22. Francisco LM, Salinas VH, Brown KE, Vanguri VK, Freeman GJ, Kuchroo VK, Sharpe AH. PD-L1 regulates the development, maintenance, and function of induced regulatory T cells. The Journal of experimental medicine. 2009; 206:3015–3029. [PubMed: 20008522]
23. Gatza E, Wahl DR, Opipari AW, Sundberg TB, Reddy P, Liu C, Glick GD, Ferrara JL. Manipulating the bioenergetics of alloreactive T cells causes their selective apoptosis and arrests graft-versus-host disease. Sci Transl Med. 2011; 3:67ra68.
24. Byersdorfer CA, Tkachev V, Opipari AW, Goodell S, Swanson J, Sandquist S, Glick GD, Ferrara JL. Effector T cells require fatty acid metabolism during murine graft-versus-host disease. Blood. 2013; 122:3230–3237. [PubMed: 24046012]
25. Hildeman DA. Regulation of T-cell apoptosis by reactive oxygen species. Free Radic Biol Med. 2004; 36:1496–1504. [PubMed: 15182852]
26. Hildeman DA, Mitchell T, Teague TK, Henson P, Day BJ, Kappler J, Marrack PC. Reactive oxygen species regulate activation-induced T cell apoptosis. Immunity. 1999; 10:735–744. [PubMed: 10403648]
27. Keir ME, Freeman GJ, Sharpe AH. PD-1 regulates self-reactive CD8+ T cell responses to antigen in lymph nodes and tissues. Journal of immunology. 2007; 179:5064–5070.
28. Cooke KR, Kobzik L, Martin TR, Brewer J, Delmonte J Jr, Crawford JM, Ferrara JL. An experimental model of idiopathic pneumonia syndrome after bone marrow transplantation: I. The roles of minor H antigens and endotoxin. Blood. 1996; 88:3230–3239. [PubMed: 8963063]
29. Ali N, Flutter B, Sanchez Rodriguez R, Sharif-Paghaleh E, Barber LD, Lombardi G, Nestle FO. Xenogeneic graft-versus-host-disease in NOD-scid IL-2Rgammanull mice display a T-effector memory phenotype. PloS one. 2012; 7:e44219. [PubMed: 22937164]
30. King MA, Covassin L, Brehm MA, Racki W, Pearson T, Leif J, Laning J, Fodor W, Foreman O, Burzenski L, Chase TH, Gott B, Rossini AA, Bortell R, Shultz LD, Greiner DL. Human peripheral blood leucocyte non-obese diabetic-severe combined immunodeficiency interleukin-2 receptor gamma chain gene mouse model of xenogeneic graft-versus-host-like disease and the role of host major histocompatibility complex. Clinical and experimental immunology. 2009; 157:104–118. [PubMed: 19659776]
31. Dickinson BC, Chang CJ. A targetable fluorescent probe for imaging hydrogen peroxide in the mitochondria of living cells. J Am Chem Soc. 2008; 130:9638–9639. [PubMed: 18605728]
32. Cantor JM, Ginsberg MH. CD98 at the crossroads of adaptive immunity and cancer. Journal of cell science. 2012; 125:1373–1382. [PubMed: 22499670]
33. Haynes BF, Hemler M, Cotner T, Mann DL, Eisenbarth GS, Strominger JL, Fauci AS. Characterization of a monoclonal antibody (5E9) that defines a human cell surface antigen of cell activation. Journal of immunology. 1981; 127:347–351.
34. Lorvik KB, Haabeth OA, Clancy T, Bogen B, Corthay A. Molecular profiling of tumor-specific T1 cells activated in vivo. Oncoimmunology. 2013; 2:e24383. [PubMed: 23762808]
35. Millrud CR, Mansson Kvarnhammar A, Uddman R, Bjornsson S, Riesbeck K, Cardell LO. The activation pattern of blood leukocytes in head and neck squamous cell carcinoma is correlated to survival. PloS one. 2012; 7:e51120. [PubMed: 23251433]
36. Paz Morante M, Briones J, Canto E, Sabzevari H, Martino R, Sierra J, Rodriguez-Sanchez JL, Vidal S. Activation-associated phenotype of CD3 T cells in acute graft-versus-host disease. Clinical and experimental immunology. 2006; 145:36–43. [PubMed: 16792671]
37. Shipkova M, Wieland E. Surface markers of lymphocyte activation and markers of cell proliferation. Clinica chimica acta; international journal of clinical chemistry. 2012; 413:1338–1349.

38. Butte MJ, Keir ME, Phamduy TB, Sharpe AH, Freeman GJ. Programmed death-1 ligand 1 interacts specifically with the B7-1 costimulatory molecule to inhibit T cell responses. Immunity. 2007; 27:111–122. [PubMed: 17629517]
39. Balaban RS, Nemoto S, Finkel T. Mitochondria, oxidants, and aging. Cell. 2005; 120:483–495. [PubMed: 15734681]
40. Okazaki T, Chikuma S, Iwai Y, Fagarasan S, Honjo T. A rheostat for immune responses: the unique properties of PD-1 and their advantages for clinical application. Nature immunology. 2013; 14:1212–1218. [PubMed: 24240160]
41. Day BJ, Fridovich I, Crapo JD. Manganic porphyrins possess catalase activity and protect endothelial cells against hydrogen peroxide-mediated injury. Arch Biochem Biophys. 1997; 347:256–262. [PubMed: 9367533]
42. Patel M. Inhibition of neuronal apoptosis by a metalloporphyrin superoxide dismutase mimic. J Neurochem. 1998; 71:1068–1074. [PubMed: 9721731]
43. Laniewski NG, Grayson JM. Antioxidant treatment reduces expansion and contraction of antigen-specific CD8+ T cells during primary but not secondary viral infection. J Virol. 2004; 78:11246–11257. [PubMed: 15452243]
44. Wherry EJ, Ha SJ, Kaech SM, Haining WN, Sarkar S, Kalia V, Subramaniam S, Blattman JN, Barber DL, Ahmed R. Molecular signature of CD8+ T cell exhaustion during chronic viral infection. Immunity. 2007; 27:670–684. [PubMed: 17950003]
45. Blatt NB, Boitano AE, Lyssiotis CA, Opipari AW Jr, Glick GD. Bz-423 superoxide signals apoptosis via selective activation of JNK, Bak, and Bax. Free Radic Biol Med. 2008; 45:1232–1242. [PubMed: 18718527]
46. Sundberg TB, Swenson L, Wahl DR, Opipari AW Jr, Glick GD. Apoptotic signaling activated by modulation of the F0F1-ATPase: implications for selective killing of autoimmune lymphocytes. J Pharmacol Exp Ther. 2009; 331:437–444. [PubMed: 19706792]
47. Petrovas C, Price DA, Mattapallil J, Ambrozak DR, Geldmacher C, Cecchinato V, Vaccari M, Tryniszewska E, Gostick E, Roederer M, Douek DC, Morgan SH, Davis SJ, Franchini G, Koup RA. SIV-specific CD8+ T cells express high levels of PD1 and cytokines but have impaired proliferative capacity in acute and chronic SIVmac251 infection. Blood. 2007; 110:928–936. [PubMed: 17440051]
48. Zelinskyy G, Myers L, Dietze KK, Gibbert K, Roggendorf M, Liu J, Lu M, Kraft AR, Teichgraber V, Hasenkrug KJ, Dittmer U. Virus-specific CD8+ T cells upregulate programmed death-1 expression during acute friend retrovirus infection but are highly cytotoxic and control virus replication. Journal of immunology. 2011; 187:3730–3737.
49. Taylor PA, Panoskaltsis-Mortari A, Freeman GJ, Sharpe AH, Noelle RJ, Rudensky AY, Mak TW, Serody JS, Blazar BR. Targeting of inducible costimulator (ICOS) expressed on alloreactive T cells down-regulates graft-versus-host disease (GVHD) and facilitates engraftment of allogeneic bone marrow (BM). Blood. 2005; 105:3372–3380. [PubMed: 15618467]
50. Watanabe S, Ogawa S, Hara Y, Tanabe K, Toma H, Abe R. Expression level of costimulatory receptor ICOS is critical for determining the polarization of helper T cell function. Transplant immunology. 2006; 15:255–263. [PubMed: 16635747]
51. Byersdorfer CA. The role of Fatty Acid oxidation in the metabolic reprograming of activated t-cells. Frontiers in immunology. 2014; 5:641. [PubMed: 25566254]
52. Nishimura H, Nose M, Hiai H, Minato N, Honjo T. Development of lupus-like autoimmune diseases by disruption of the PD-1 gene encoding an ITIM motif-carrying immunoreceptor. Immunity. 1999; 11:141–151. [PubMed: 10485649]
53. Nishimura H, Okazaki T, Tanaka Y, Nakatani K, Hara M, Matsumori A, Sasayama S, Mizoguchi A, Hiai H, Minato N, Honjo T. Autoimmune dilated cardiomyopathy in PD-1 receptor-deficient mice. Science. 2001; 291:319–322. [PubMed: 11209085]
54. Jackson SH, Devadas S, Kwon J, Pinto LA, Williams MS. T cells express a phagocyte-type NADPH oxidase that is activated after T cell receptor stimulation. Nature immunology. 2004; 5:818–827. [PubMed: 15258578]

55. Purushothaman D, Sarin A. Cytokine-dependent regulation of NADPH oxidase activity and the consequences for activated T cell homeostasis. The Journal of experimental medicine. 2009; 206:1515–1523. [PubMed: 19546249]

56. Kwon J, Shatynski KE, Chen H, Morand S, de Deken X, Miot F, Leto TL, Williams MS. The nonphagocytic NADPH oxidase Duox1 mediates a positive feedback loop during T cell receptor signaling. Sci Signal. 2010; 3:ra59. [PubMed: 20682913]

57. Perl A, Gergely P Jr, Puskas F, Banki K. Metabolic switches of T-cell activation and apoptosis. Antioxid Redox Signal. 2002; 4:427–443. [PubMed: 12215210]

58. Sena LA, Li S, Jairaman A, Prakriya M, Ezponda T, Hildeman DA, Wang CR, Schumacker PT, Licht JD, Perlman H, Bryce PJ, Chandel NS. Mitochondria are required for antigen-specific T cell activation through reactive oxygen species signaling. Immunity. 2013; 38:225–236. [PubMed: 23415911]

59. Kaminski MM, Sauer SW, Kaminski M, Opp S, Ruppert T, Grigaravicius P, Grudnik P, Grone HJ, Krammer PH, Gulow K. T cell activation is driven by an ADP-dependent glucokinase linking enhanced glycolysis with mitochondrial reactive oxygen species generation. Cell Rep. 2012; 2:1300–1315. [PubMed: 23168256]

60. Kaminski M, Kiessling M, Suss D, Krammer PH, Gulow K. Novel role for mitochondria: protein kinase Ctheta-dependent oxidative signaling organelles in activation-induced T-cell death. Mol Cell Biol. 2007; 27:3625–3639. [PubMed: 17339328]

61. Hildeman DA, Mitchell T, Aronow B, Wojciechowski S, Kappler J, Marrack P. Control of Bcl-2 expression by reactive oxygen species. Proc Natl Acad Sci U S A. 2003; 100:15035–15040. [PubMed: 14657380]

62. Dong H, Strome SE, Salomao DR, Tamura H, Hirano F, Flies DB, Roche PC, Lu J, Zhu G, Tamada K, Lennon VA, Celis E, Chen L. Tumor-associated B7-H1 promotes T-cell apoptosis: a potential mechanism of immune evasion. Nature medicine. 2002; 8:793–800.

63. Tome ME, Johnson DB, Samulitis BK, Dorr RT, Briehl MM. Glucose 6-phosphate dehydrogenase overexpression models glucose deprivation and sensitizes lymphoma cells to apoptosis. Antioxid Redox Signal. 2006; 8:1315–1327. [PubMed: 16910779]

64. Phillips DC, Woollard KJ, Griffiths HR. The anti-inflammatory actions of methotrexate are critically dependent upon the production of reactive oxygen species. Br J Pharmacol. 2003; 138:501–511. [PubMed: 12569075]

65. Zamzami N, Marchetti P, Castedo M, Decaudin D, Macho A, Hirsch T, Susin SA, Petit PX, Mignotte B, Kroemer G. Sequential reduction of mitochondrial transmembrane potential and generation of reactive oxygen species in early programmed cell death. The Journal of experimental medicine. 1995; 182:367–377. [PubMed: 7629499]

66. Lassegue B, Griendling KK. Mycophenolic acid is a new Nox2 inhibitor. Hypertension. 2007; 49:25–26. [PubMed: 17101843]

67. Honeychurch J, Alduaij W, Azizyan M, Cheadle EJ, Pelicano H, Ivanov A, Huang P, Cragg MS, Illidge TM. Antibody-induced nonapoptotic cell death in human lymphoma and leukemia cells is mediated through a novel reactive oxygen species-dependent pathway. Blood. 2012; 119:3523–3533. [PubMed: 22354003]

68. Sa G, Das T, Moon C, Hilston CM, Rayman PA, Rini BI, Tannenbaum CS, Finke JH. GD3, an overexpressed tumor-derived ganglioside, mediates the apoptosis of activated but not resting T cells. Cancer Res. 2009; 69:3095–3104. [PubMed: 19276353]

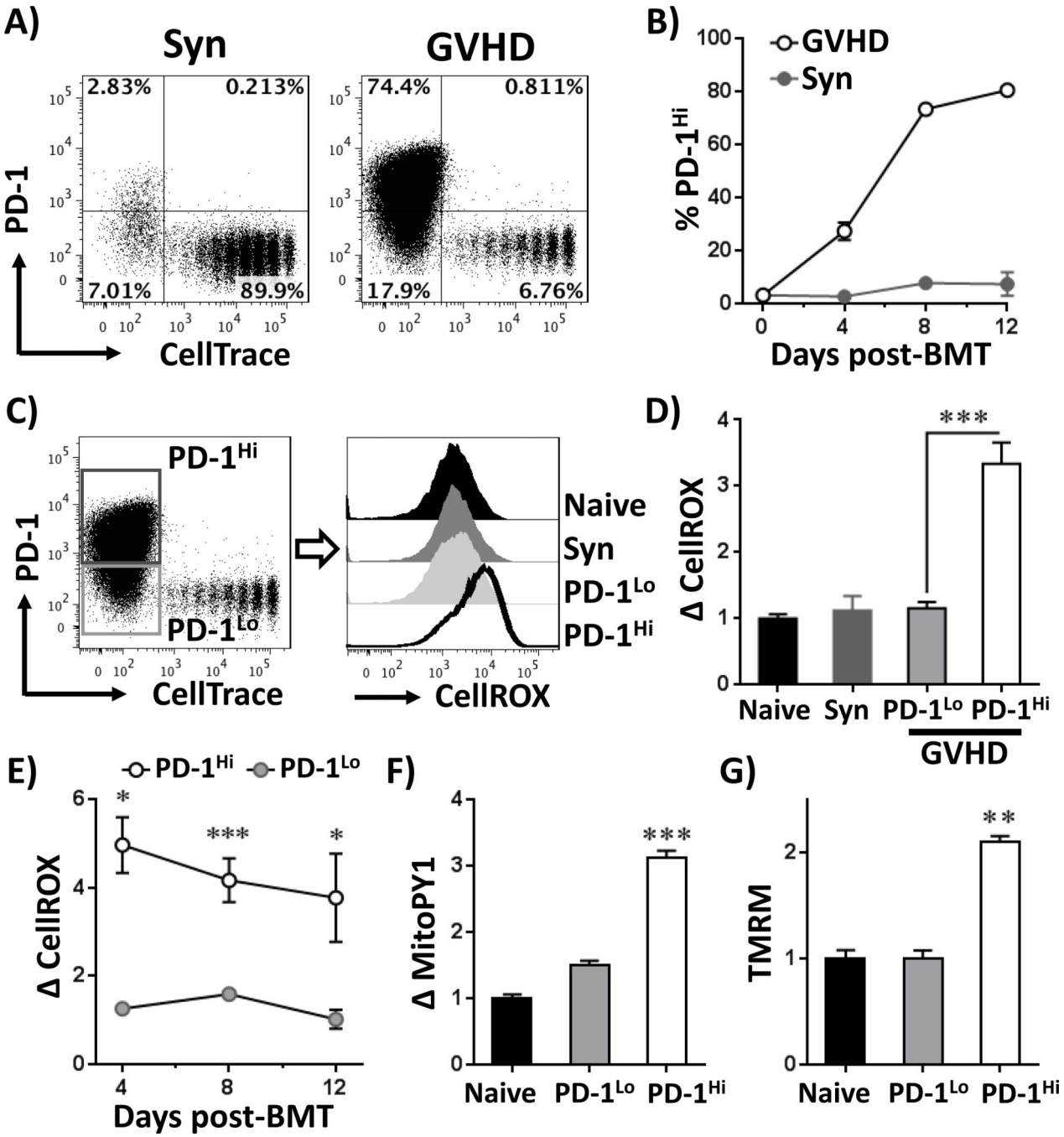

Figure 1. Alloreactive T cells concomitantly increase PD-1 expression and cellular ROS levels

A, B6-Ly5.2 donor T cells (CD45.1$^+$) were labeled with CellTrace Violet dye (CellTrace) and transferred to irradiated B6D2F1 (allogeneic = GVHD) or syngeneic B6 (Syn) recipients as detailed in Materials and Methods. T cells were recovered from spleens on day 7 post-BMT and stained for PD-1. Plots are gated on CD45.1$^+$, TCR-β$^+$ CD8a$^+$ cells. B, The percentage of PD-1^{Hi} cells was quantitated in donor CD8 T cells on days 4, 8 and 12 following syngeneic (gray circles) or allogeneic (open circles) transplantation. C, B6-Ly5.2 donor T cells were stained for PD-1 similar to *A*, followed by assessment of total cellular

ROS using CellROX Deep Red (CellROX). D, CellROX median fluorescence intensity (MFI) was quantitated in T cells recovered from multiple recipients and compared to MFI values in un-manipulated (naive) T cells, which was set to a relative value of 1. Gating and analysis for PD-$1^{Hi/Lo}$ as shown in *C*, n = 4–6 mice per group. E, ROS levels were measured in PD-1^{Lo} and PD-1^{Hi} (as gated in C) donor CD8 T cells on days 4, 8 and 12 post-BMT and expressed as the difference in CellROX MFI compared to naïve T cells, n = 5–7 mice per group. Mitochondrial ROS levels (F) and mitochondrial transmembrane potential (G) were measured using MitoPY1 probe and TMRM, respectively. For both MitoPY1 and TMRM, the MFI was quantitated in T cells recovered from multiple recipients and compared to MFI values in un-manipulated (naive) T cells, which was set to a relative value of 1. Gating on PD-1^{Hi} and PD-1^{Lo} cell populations as shown in *C*. n = 3–5 mice per group. * $p < 0.01$, ** $p < 0.001$, *** $p < 0.0001$

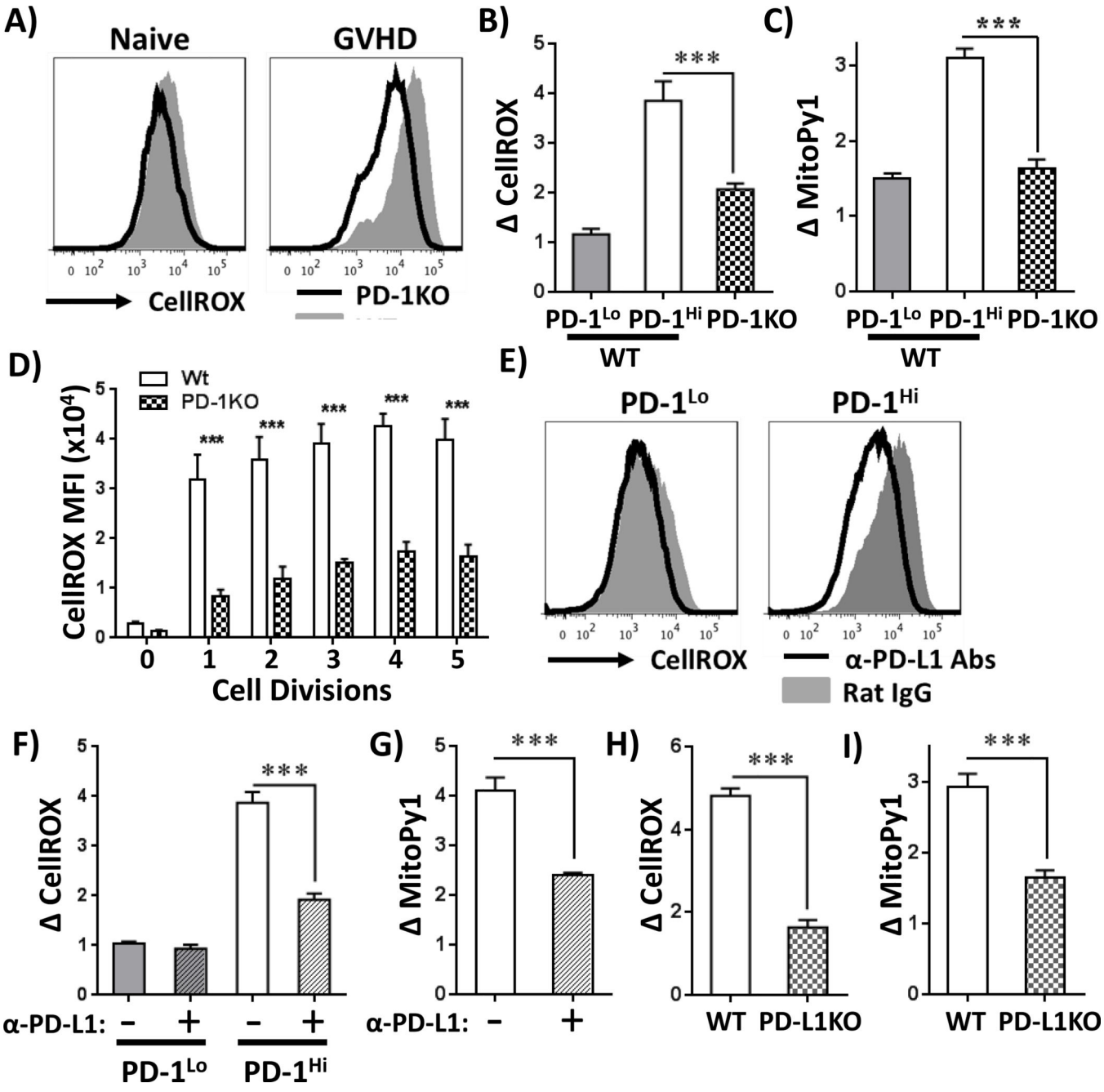

Figure 2. PD-1 controls ROS levels in allogeneic T cells

A, Wild-type (WT, gray histograms) or PD-1 knockout (PD-1KO, solid black line) T cells were transferred to B6D2F1 recipients and ROS levels measured on day 7 post-transplant. WT PD-1^{Hi} and PD-1^{Lo} T cells were gated as in Figure 1C, PD-1KO cells were gated on CellTrace^{Lo} cells (> 8 divisions). B-C, Changes in CellROX (B) or MitoPy1 (C) were averaged in WT PD-1^{Lo}, WT PD-1^{Hi} or PD-1KO T cells from multiple recipients (n = 3–5 mice/group), gating as in *A*. D, WT or PD-1 KO T cells were stimulated *in vitro* with B6D2F1 splenocytes and total cellular ROS levels measured as a function of cell division. E, Following B6 into F1 transplantation, recipients received anti-PD-L1 blocking antibodies (or

isotype-matched Rat IgG control) on days 1, 3 and 6. ROS levels were then measured in PD-1^{Lo} and PD-1^{Hi} CD8 donor T cells recovered on day 7. F, Average changes in CellROX MFI were quantitated in donor PD-1^{Hi} or PD-1^{Lo} T cells from multiple recipients treated with anti-PD-L1 or isotype control antibodies. n = 6 mice/group. Primary data as shown in Figure 2E. G, Average changes in MitoPy1 MFI was quantitated in donor PD-1^{Hi} T cells from multiple animals, n = 6 mice/group. H-I, CellTrace-labeled C3H.SW (Ly9.1^{+}) T cells were transferred to irradiated WT or PD-L1 knockout (PD-L1KO) recipients and donor T cells recovered on day 10 post-BMT. Relative CellROX (H) or MitoPy1 (I) MFI values were then quantitated in Ly9.1^{+}, TCR-β^{+}, $CD8^{+}$, CellTrace^{Lo}, PD-1^{Hi} T cells from multiple recipients, n = 3–5 mice/group. All gating for PD-1^{Hi} or PD-1^{Lo} subsets was done similar to that shown in Figure 1C. ***$p < 0.001$

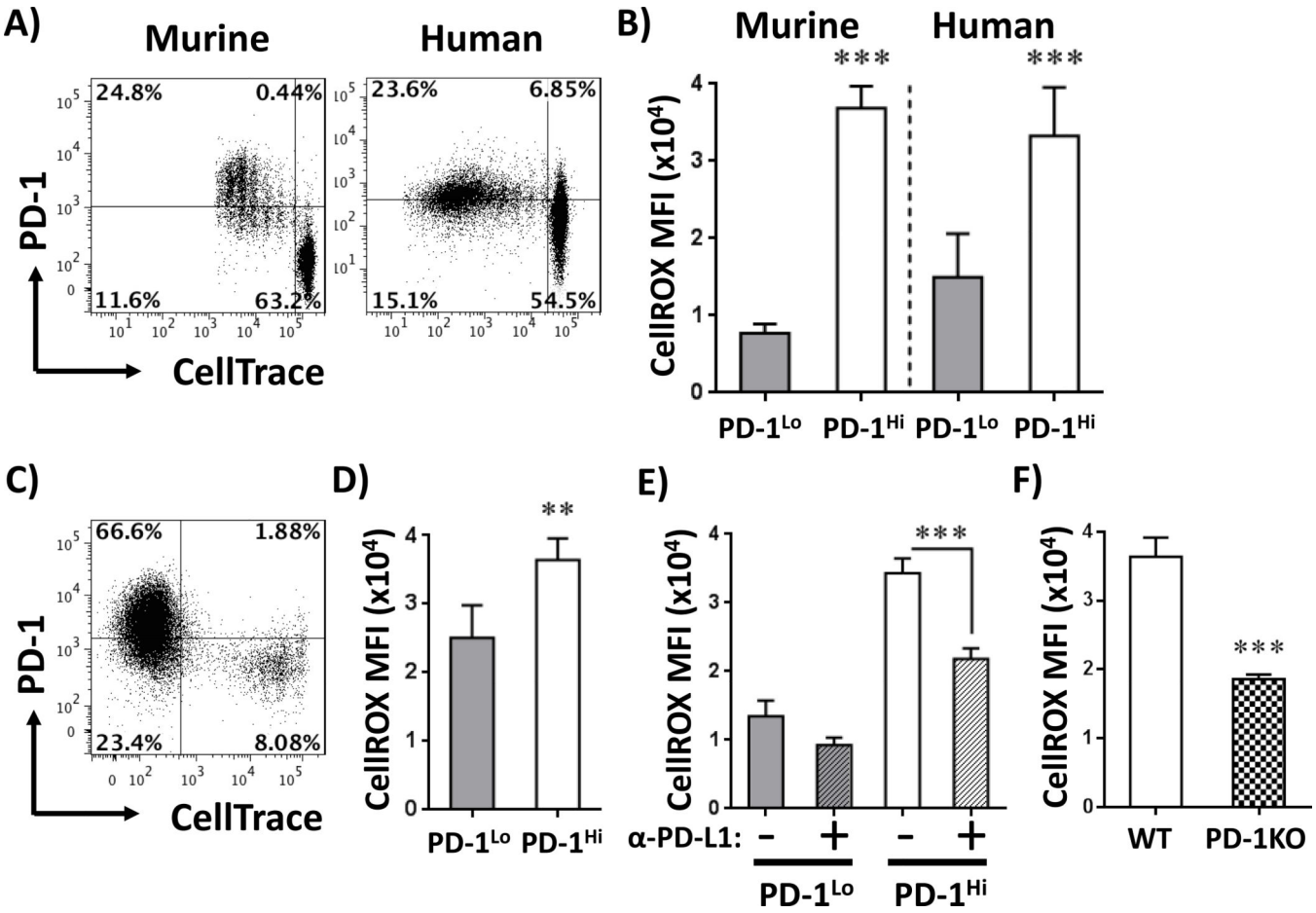

Figure 3. PD-1 controls ROS levels in human T cells

A, Murine B6-Ly5.2 or purified human T cells were labeled with CellTrace and co-cultured with F1 splenocytes (murine) or non-T, peripheral blood mononuclear cells (PBMCs) from unrelated donors (human). At harvest, cells were stained with cell surface markers and PD-1 levels quantitated. Murine plots are gated on CD45.1^{+}, TCR-β^{+} CD8a^{+} cells; human plots represent CD3^{+}CD8a^{+} cells. B, ROS levels were measured in well-divided murine or human PD-1^{Lo} (lower left quadrant) versus PD-1^{Hi} (upper left quadrant) CD8^{+} T cells as outlined in *A.* Graphs represent independent data from 6 murine and 8 human samples. C, Human PBMCs were labeled with CellTrace and injected into immunodeficient (NSG) mice in a model of xenogeneic GVHD. Cells were harvested between day 12 and 14, gated on human CD3^{+}, CD8^{+} and stained for PD-1. D, ROS levels were analyzed in human CellTrace^{Lo}PD-1^{Lo} (lower left quadrant) versus PD-1^{Hi} (upper left quadrant) CD8 T cells during xenogeneic GVHD as in *C*, n=8 NSG recipients/group. F, Human MLR cultures were treated with anti-PD-L1 antibodies on days 0, 3, and 6 and ROS levels measured in PD-1^{Lo} versus PD-1^{Hi} CD8 T cells eight hours after the final treatment, with gating for PD-1^{Lo} versus PD-1^{Hi} subsets similar to Figure 3A. F, Murine WT or PD-1KO T cells were cultured with F1 splenocytes, followed by staining for ROS levels as in Figure 3B. n=5–6 mice/group. **p< 0.001, ***p <0.0001

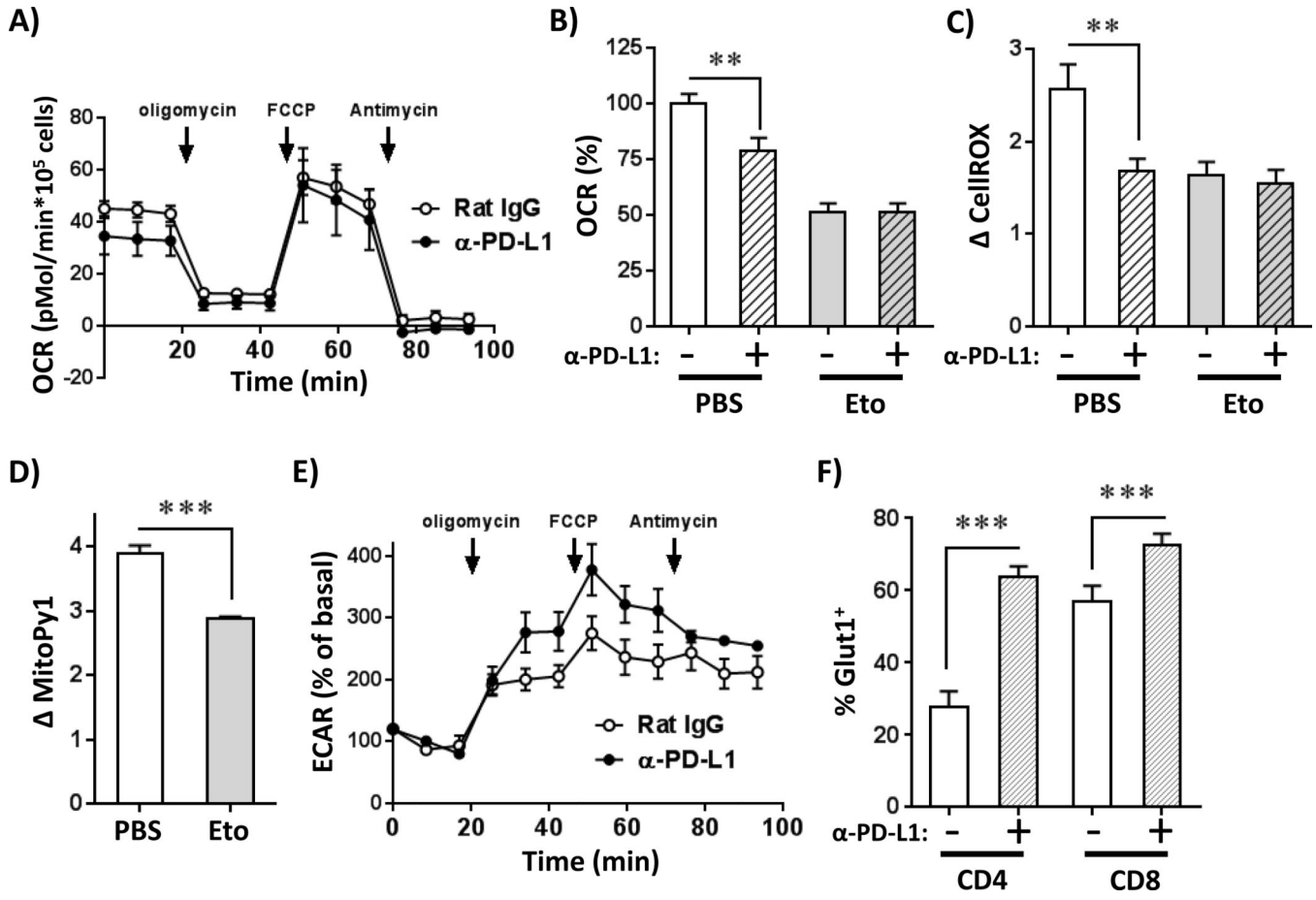

Figure 4. Inhibition of FAO negates PD-1 driven changes in ROS levels

A, B6 into F1 recipients were treated with anti-PD-L1 blocking antibodies (or Rat IgG control) as in Figure 2C. On day 7 post-transplant, CD45.1^{+} donor T cells were isolated and oxygen consumption rates (OCR) quantitated using a Seahorse XF24 metabolic analyzer. B, Baseline OCR values were measured in alloreactive T cells from multiple recipients, with data combined from two independent experiments. Primary data as shown in Figure 4A, n = 8–9 mice/group. In some cases, T cells were pretreated with 100 μM etomoxir for 15 minutes prior to analysis (PBS as negative control). C-D, Day 7 PD-1^{Hi} donor T cells, from B6 into F1 transplants were treated with etomoxir for 15 minutes, then evaluated for changes in (C) total cellular ROS or (D) mitochondrial H_2O_2 levels (using MitoPy1), n = 8–9 mice/group. E, Cells were recovered as in Figure 4A and extracellular acidification rates (ECAR) measured using Seahorse XF24. F, Following B6 into F1 BMT, day 7 donor CellTrace^{Lo} CD4^{+} or CD8^{+} T cells were stained for GLUT1 expression level by flow cytometry. *p < 0.05, **p <0.01, ***p <0.001.

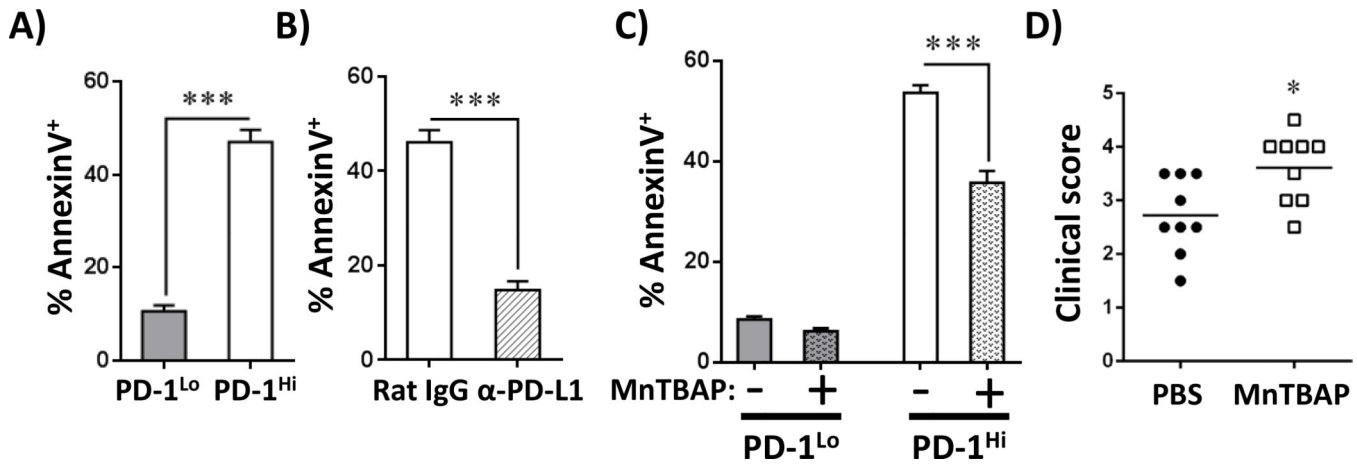

Figure 5. ROS levels mediate PD-1-induced apoptosis

A, The percentage of AnnexinV^{+} cells was quantitated in CellTrace^{Lo} PD-1^{Lo} versus CellTrace^{Lo} PD-1^{Hi} donor T cells 7 days after B6 into F1 BMT. B, Similar to *A*, AnnexinV staining was assessed in PD-1^{Hi} CD8T cells +/− blockade with anti-PD-L1 antibodies (Rat IgG as control). C, C3H.SW into B6 recipients were treated with the antioxidant MnTBAP on day 9 post-BMT and AnnexinV positivity assessed in PD-1^{Hi} CD8 T cells the following day. Data represent the percentage of AnnexinV^{+} cells in PD-1^{Lo} or PD-1^{Hi} CD8 T cell subsets, averaged from 5 mice/group. D, C3H.SW into B6 recipient mice were treated with 5 doses of MnTBAP and clinical scores assessed one week after the final treatment. In all cases, gating for PD-1^{Lo} versus PD-1^{Hi} performed similarly to Figure 1C. *$p < 0.05$; ***$p < 0.001$

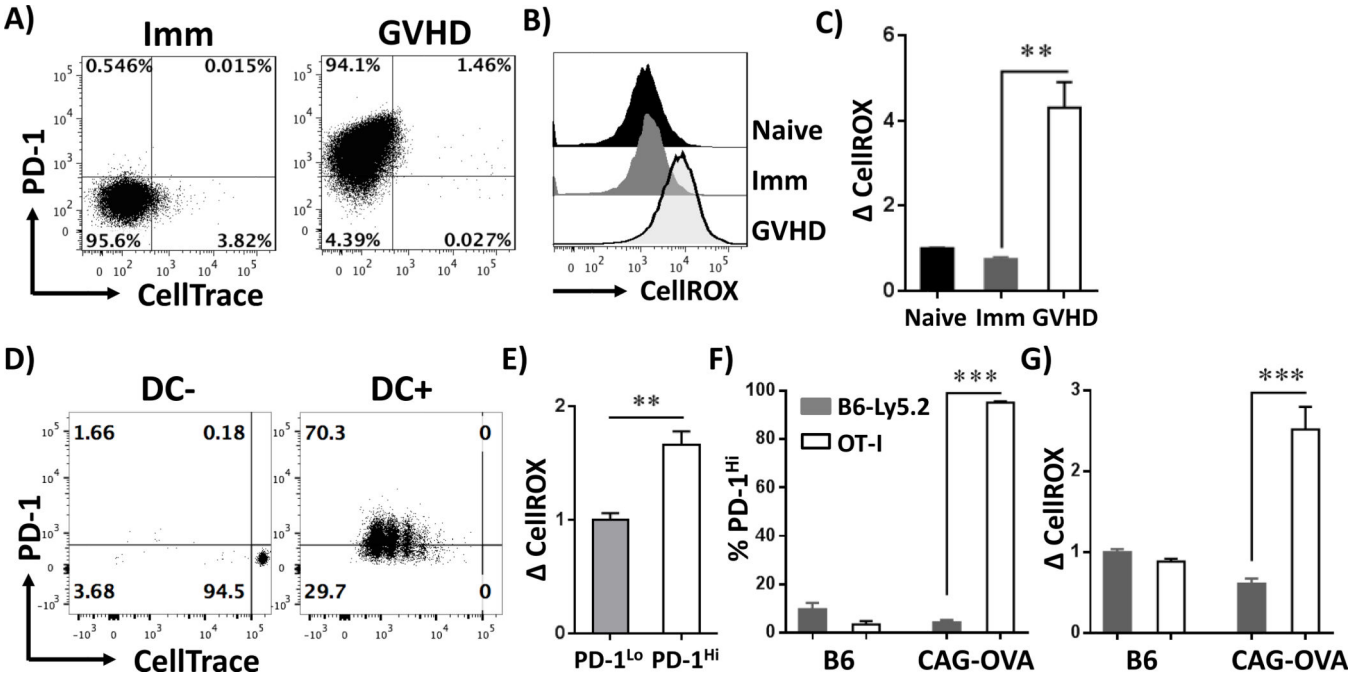

Figure 6. PD-1^{Hi}, ROS^{Hi} phenotype is specific to allogeneic T cells and requires antigenic stimulation

A, CellTrace-labeled OT-I T cells (CD45.2^{+}) were transferred into 1) syngeneic B6-Ly5.2 recipients followed by dendritic cell immunization (Imm) or 2) irradiated CAG-OVA mice (GVHD). T cells were recovered on day 7 and stained for PD-1 expression. Plots are gated on CD45.2^{+}, TCR-β^{+} CD8^{+} cells. B, Total cellular ROS levels were quantitated in OT-I T cells from naïve, immunized or GVHD recipients (gating as shown in Figure 6A). C, CellROX MFI values from multiple recipients were normalized to the level observed in un-manipulated OT-I cells. D, CellTrace-labeled OT-I T cells were transferred into syngeneic B6-Ly5.1 recipients, followed by dendritic cell immunization (DC+) or PBS control (DC-). 3 days post-immunization, cells were harvested and stained for PD-1 levels versus cell division status. Plots are gated as in *A*. E, CellROX staining was quantitated in divided, PD-1^{Lo} (Figure 6D, left lower quadrant) versus PD-1^{Hi} (upper left quadrant) cells from multiple recipients. CellROX staining was set a relative value of 1 in PD-1^{Lo} cells. F-G, OT-I (CD45.1^{+}, CD45.2^{+}) T cells were co-transferred with B6-Ly5.2 (CD45.1^{+}) T cells into irradiated syngeneic (B6) or allogeneic (CAG-OVA) recipients. T cells were recovered on day 7 and stained for PD-1 expression (D) or probed with CellROX to quantitate cellular ROS levels (E). n = 3 recipients/group. **p < 0.01, ***p <0.001

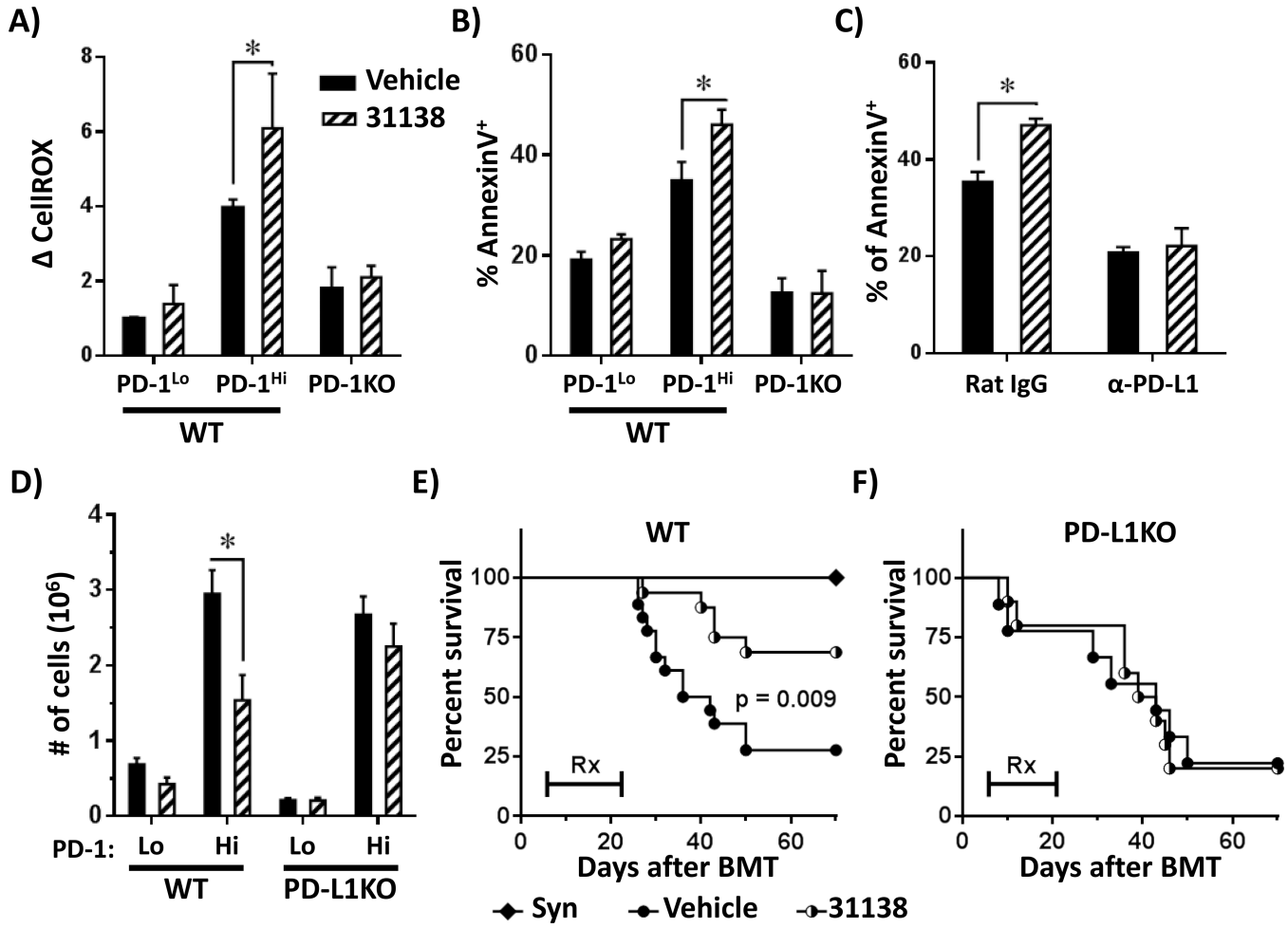

Figure 7. PD-1 driven ROS are required for subsequent metabolic inhibition

WT or PD-1KO T cells were transferred to F1 hosts and recipient mice treated with LYC-31138 (or vehicle control) on day 7 post-BMT. Changes in total ROS (A) or the percentage of AnnexinV$^+$ cells (B) was quantitated in WT PD-1^{Lo}, WT PD-1^{Hi} or CellTrace^{Lo} PD-1KO CD8 T cells 150 minutes after LYC-31138 treatment (n ≥ 3 mice/group). PD-1 status gated as in Figure 1C. C, B6 into F1 recipient mice were treated with anti-PD-L1 blocking antibodies (as in Figure 2E), followed by LYC-31138 treatment (or vehicle control) on day 7 post-BMT and the percentage of AnnexinV$^+$ cells quantitated 150 minutes after LYC-31138 treatment (n ≥ 3 mice/group). D, C3H.SW T cells were transferred to WT or PD-L1 deficient mice and recipients treated with 4 doses of LYC-31138 or vehicle control. Cells were harvested on day 12 post-BMT and the absolute number of PD-1^{Hi} or PD-1^{Lo} donor, CD8$^+$ T cells (Ly9.1$^+$ TCR-β$^+$) was quantitated. Gating for PD-1 subsets was performed similar to Figure 1C. Data were pooled from 2 identical experiments, n ≥ 6/group. E, C3H.SW T cells were transferred to irradiated C3H.SW (syngeneic) or WT B6 recipients. Beginning day 5 post-BMT, recipient mice received LYC-31138 (half-filled circles) or Vehicle (closed circles) every other day for a total of 9 doses. Survival was monitored up to 70 days post-transplant. F, Similar to *E*, only C3H.SW

T cells were transferred to PD-L1 knockout recipients (PD-L1KO), followed by LYC-31138 versus vehicle treatment. n = 10–12 mice per allogeneic group. *p < 0.05

Table I

Influence of PD-1 blockade on ROS levels in multiple models of GVHD

GVHD model	Method of PD-1/PD-L1 blockade	PD-1 Correlated w/ ROS level	ROS decreased w/ PD-1 blockade (% decrease)
B6 into F1	Donor PD1KO T cells	Yes	Yes (46%)
B6 into F1	Anti-PD-L1 Abs	Yes	Yes (52%)
B6 into F1	Anti-PD-L1 Abs	Yes	Yes (50%)
B6 into Balb/C	Donor PD1KO T cells	Yes	Yes (54%)
B6 into C3H.SW	Donor PD1KO T cells	Yes	Yes (43%)
C3H.SW into B6	PD-L1KO recipients	Yes	Yes (66%)
C3H/HeJ into B6	Anti-PD-L1 Abs	Yes	Yes (25%)
Balb/C into B6	PD-L1KO recipients	Yes	No
Human MLR	Anti-PD-L1 Abs	Yes	Yes (36%)
Xenogeneic GVHD		Yes	